Journal of Materials Chemistry

Cite this: J. Mater. Chem., 2012, 22, 6782

www.rsc.org/materials

PAPER

Inclusion effect of gold and copper particles in a poly(amide) matrix that contains a thiophene moiety and Si or Ge atoms in the main chain

Carmen M. González Henríquez,*[a] Claudio A. Terraza,[a] Luis H. Tagle,[a] Andrés Barriga González,[c] Ulrich G. Volkmann,[b] Alejandro L. Cabrera,[b] Esteban Ramos-Moore[b] and María J. Retamal[b]

Received 22nd November 2011, Accepted 22nd January 2012
DOI: 10.1039/c2jm16083h

Soluble pure silicon or germanium-containing poly(amide)s and their metallic composites (Cu or Au) were synthesized and characterized. Optical band gaps of pure polymer were comparable to an insulator behavior; however, the conductivity of some composites at several concentrations shows a diode-like behavior. Samples exhibit a monoclinic lattice mixed with amorphous structures. Specifically, polymer–Au composites showed distortion of this unit cell, associated with an increase in the conductance. This effect would be related to the coordination of the central atom (Si or Ge) to the incorporated metal, producing a homogeneous distribution of metallic particles within the system.

Introduction

Aromatic poly(amide)s are studied due to their excellent balance of thermal, optical and mechanical properties. Some applications related to these compounds are: hydro-gel formation for drug delivery,[1] fabrication of mirrors,[2–4] electrochromic displays,[5,6] smart windows[7–10] and earth-tone chameleon materials.[11–13] However, the poor solubility and high melting temperature are properties that hinder the processability and thus the use of these polymers in other technological applications. One of the successful approaches to improve these properties, always existing the possibility to affect some of the desirable properties of the material, is the introduction of bulky lateral substituents,[14–16] flexible alkyl side chains,[17,18] and asymmetric,[19] alicyclic[20,21] and linked structures.[22,23] In most of the cases, the improvements are related to the breaking of symmetry and the loss of regularity within the chains, which diminishes the intramolecular interactions. Also, these structural modifications decrease the inter-chain interactions due to the steric effect on the packing, mainly hydrogen bonds and dipole–dipole interactions. All these would negatively affect the overlap of atomic orbitals and therefore the electron delocalization. Thus, the incorporation of specific groups, such as a thiophene moiety, specifically the quinoidine form of this compound, is predicted to possess a near-zero band gap, a value that is related to bond length alternation along the backbone of the polymer. Due to this characteristic, the polymers may show a photovoltaic behavior.[24–26] On the other hand, the inclusion of Si–C or Ge–C bonds generally increases the solubility of the polymers and maintains the thermal stability as a consequence of the ionic character of the linkages.[27–31]

In order to enhance the mechanical, optical and electrical properties of the polymers, the inclusion of specific metals by ion implantation techniques has been suggested.[32–35] Recently, new applications for metalized polymer films and membranes have emerged in the field of organic electronics,[36] organic solar cells[37] and high-flux gas transport.[38]

We studied the inclusion of a metal (Au or Cu) in the silicon or germanium-containing poly(amide)s and their effect on the structure, morphology, electrical conductivity and optical properties of the polymer–metal composite film derivatives. For this, Raman spectroscopy, X-ray diffraction, SEM, voltage–current and optical absorbance analyses were used. The main goal of this study is to understand the perturbation of the above described properties when the metals are incorporated into the polymeric matrix.

The new poly(amide)s were successfully prepared from 2,5-thiophenedicarboxylic acid (**1**) and two different aromatic diamines (**2a–b**) with Si or Ge as a central element in their structure *via* the phosphorylation polyamidation reaction (Scheme 1). FT-IR and NMR spectra were analyzed to determine the chemical structure of the polymers. The solubility of the poly(amide)s was studied in common organic solvents. The molecular weight of the polymers was determined using ElectroSpray Ionization mass spectrometry (ESI). The glass transition temperature (T_g) and the thermal stability (TDT) were studied by Differential Scanning Calorimetry (DSC) and Thermal Gravimetric Analysis (TGA), respectively.

[a]*Pontificia Universidad Católica de Chile, Facultad de Química, P.O. Box 306, Correo 22, Santiago, Chile. E-mail: cgonzalen@uc.cl*
[b]*Pontificia Universidad Católica de Chile, Facultad de Física, P.O. Box 306, Correo 22, Santiago, Chile*
[c]*Universidad de Chile, Facultad de Ciencias Químicas y Farmacéuticas, Av. Vicuña Mackenna 20, Santiago, Chile*

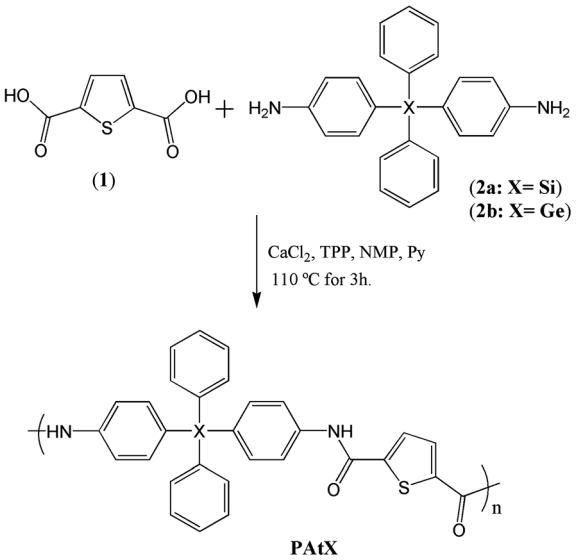

Scheme 1 Synthesis of poly(amide)s: **PAtSi** (X = Si) and **PAtGe** (X = Ge).

Experimental

Materials

2,5-Thiophenedicarboxylic acid (**1**), triphenylphosphite (TPP), dehydrated *N*-methyl-2-pyrrolidone (NMP) and pyridine (Py) were purchased from Sigma-Aldrich (Milwaukee, WI). Anhydrous calcium chloride powder was purchased from Merck (Darmstad, Germany). Tetrahydrofuran (THF) and diethyl ether (Et_2O) were dried by distillation over sodium wire, while TPP was distilled off twice from calcium hydride and stored on molecular sieves (4 Å). Bis(4-aminophenyl)diphenylsilane (**2a**) and bis(4-aminophenyl)diphenylgermane (**2b**) were prepared according to referred procedures.[39,40] Gold grains of high purity (99.95%) and copper (sheet material of 0.01″ thickness) were supplied by Electronic Space Products International (ESPI).

Measurements

The samples were analyzed with the following equipment: the infrared spectra were measured on a Perkin-Elmer FT-IR-1310 spectrometer. ^{135}Dept, ^{1}H, ^{13}C and ^{29}Si NMR analyses were recorded on a Bruker 400 MHz spectrometer in DMSO-d_6 as solvent, using tetramethylsilane (TMS) as an internal standard. Non-modified carbons in ^{135}dept analysis are shown with an asterisk over their chemical shift. Elemental analyses (EA) were carried out on a Fisson EA-1108 instrument. Molecular weight of the polymers was determined by Liquid Chromatography-Mass Spectrometry (LC-MS). All experiments were performed on a HPLC Agilent 1100 (Agilent Technologies Inc., CA, USA), which was coupled to an ESI-IT Esquire 400 (Bruker Daltonik GmbH, Germany). The instruments were processed using the softwares ChemStation for LC 3D Rev. A.10.02 (Agilent Technologies Inc., CA, USA) and EsquireControl 5.2 (Bruker Daltonik GmbH, Germany). Phenomenex Luna (C18, 150 × 4.6 mm, 5 μm particles, and 100 Å pores) was used as a column to verify the fragmentation of the polymers. Poly(amide)s were dissolved in 1 mL of acetone and 20 μL of this solution was used to perform the chromatography studies. The drying gas was nitrogen (flow 10.0 L min^{-1}, 325 °C) and the nebulizer pressure was set to 30 psi (206842.8 Pa). Mass spectra were acquired in negative and positive modes. Absorption spectra of the polymers were recorded with an Agilent 8453 diode array spectrophotometer and the band gap energy (E_g) of the compounds was calculated from their adsorption edges. The spectra were recorded by using DMSO at 25 °C. The fluorescence spectra of the polymer solution in 10 μL of DMSO and 2.9 mL of acetone were obtained by a Perkin Elmer (Model LS-55) luminescence spectrometer equipped with a 7.3 W/50 Hz xenon source. DSC traces were recorded on a Mettler Toledo, DSC 821e differential scanning calorimetric from the second cycle of heating and the thermal degradation temperatures in a TGA/SDTA 851e Mettler Toledo thermobalance. Both analyses were recorded at a heating rate of 20 °C min^{-1} under nitrogen atmosphere. The structural and vibration properties of the polymers and polymer–metal composite films were characterized by Raman spectroscopy with a LabRam 010 instrument from ISA equipped with a 5.5 mW HeNe laser beam (633 nm). The Raman microscope uses a back-scattering geometry, where the incident beam is linearly polarized at 500 : 1 ratio. The objective lens of the microscope was an Olympus Mplan 100× (numerical aperture 0.9), which provides sufficient distance between the objective and the samples. The integration time was 25 s for all samples with an accumulation of 5 s. X-Ray diffraction patterns of polymers were taken at room temperature with a Bruker D-8 Advanced Diffractometer, using an X-ray tube with a copper anode (λ (CuKα) = 0.154 nm). The diffraction patterns were obtained in the usual θ–2θ geometry. The X-ray tube was operated at 40 kV and 40 mA. The goniometer was swept between 5° and 140° at 0.02° s^{-1} step over the whole interval. The diffracted X-rays were detected with a scintillation detector. Two-point current–voltage measurement was performed using the electronic tester RT66B from Radiant Technologies Inc. (Scheme 2b). The voltage was varied from 0 to 10 V, and then from 0 to −10 V, in steps of 0.2 V, and the measuring time per step (soak time) was 0.1 s.

The morphology of the polymer–metal composite was examined with a scanning electron microscope (SEM), model LEO 1420VP, 100 μA beam current and a working distance of 12–14 mm. The microscope was operated at high vacuum (system vacuum ~10^{-6} mbar and chamber 10^{-3} mbar). The preparation of polymer–metallic composites was carried out using 5.4 mg of polymer dissolved in 60 μL of DMSO. This solution was distributed on a metallic substrate (Cu or Au) with a spin coater, and afterwards the solvent was removed by a soft baking at 60 °C in a vacuum.

To study the inclusion effect of the metal into a polymer matrix and its electrical behavior it was necessary to change the polymer concentration, maintaining the thickness of the metallic film constant. Thus, metal films were obtained by evaporation of gold grains with a purity of 99.95% from ESPI (Electronic Space Products International) by Physical Vapor Deposition (PVD) in high vacuum at room temperature on glass substrates. Film thickness was controlled during the evaporation process with an Edwards film thickness monitor (model N° FTM5). The gold film thickness was 50 nm. On top of the metal film, the polymer

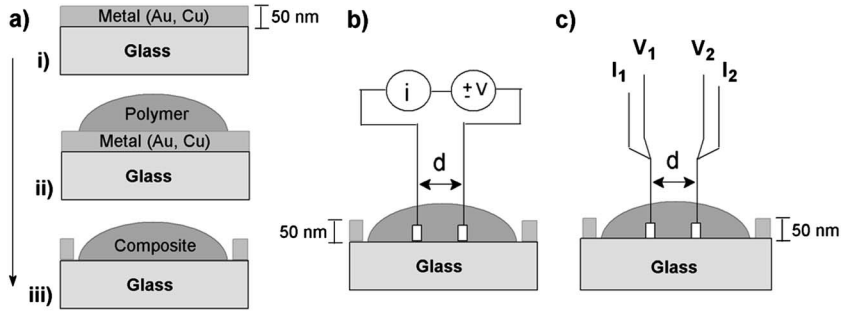

Scheme 2 (a) Inclusion procedure to segregate different metals (Au or Cu) into the polymeric systems, using a sequence of i–ii–iii and (b) experimental setup to measure the *I–V* curves. The electrodes separated by 2 mm (d) are touching the glass substrate and (c) "four point methods", with a distance between the two points of 2.5 mm (d).

was deposited by spin coating using rotation velocity ramps: 500 rpm about 10 s and 1600 rpm for 10 s.

To characterize the site percolation produced by the metal on the polymer matrix, it is necessary to verify the displacement of the gold plasmon, which is related to the absorption spectrum and electrical conductivity of the polymer–metal composites. These optical measurements were carried out by using a UV-visible spectrophotometer (UV-2450 Shimadzu) and scanning the spectra between 200 and 800 nm at the resolution of 1 nm using barium sulfate as a standard compound. To determine the resistance and conductivity in the composite films a four point probe system, connected to a multimeter (Keithley, Model 2000-200), was utilized (Scheme 2c).

Poly(amide)s synthesis

Polymerizations were developed by using the Yamazaki methodology[41,42] (Scheme 1). A typical procedure is described as follows: a mixture of 2,5-thiophenedicarboxylic acid (**1**) (0.21 g, 1.22 mmol) and bis(4-aminophenyl)diphenylsilane (**2a**) (0.45 g, 1.22 mmol), 0.3 g of $CaCl_2$, 0.9 mL of TPP, 0.8 mL of pyridine and 1.5 mL of NMP was heated while stirring at 120 °C for 3 h until the solution became dark. The resulting brown oil was extracted twice with chloroform. This organic portion was washed with HCl aq. (10%), NaOH aq. (10%), pure water and finally dried over anhydrous $MgSO_4$, filtered and the solvent evaporated. The polymer (**PatSi**) was dried until a constant mass was reached and then characterized.

When bis(4-amino)diphenylgermane (**2b**) was used as the diamine, the polymer obtained was designated as **PatGe**.

PAtSi: yield: 73%. IR (KBr, cm^{-1}): 3239 (N-H), 3071, 2957 (C-H arom.), 1662 (C=O), 1592, 1502, 1474 (C=C arom.), 1238 (Si-C arom.), 1118 (C-S-C), 814 (*p*-subst. arom.), 756 and 694 (*mono*-subst. arom.). ^{1}H NMR (DMSO-d_6): 10.31 (s, 2H, NH), 7.81–7.79 and 7.72–7.70 (dd, 2H, Ar(H)-S), 7.55–6.71 ppm (m, 18H, Ar(H)-Si). ^{13}C NMR (DMSO-d_6): 174.3 (C=O), 157.8, 138.9, 137.0*, 134.4, 132.7*, 129.8*, 129.4, 129.1*, 128.3*, 120.8* ppm. ^{29}Si NMR (DMSO-d_6): −14.9 ppm. $(C_{30}H_{22}N_2O_2SSi)(502.48)_n$: calcd C 71.70%, H 4.38%, N 5.58%; found C 71.26%, H 4.13%, N 5.35%.

PAtGe: yield: 70%. IR (KBr, cm^{-1}): 3226 (N-H), 3070, 2959 (C-H arom.), 1661 (C=O), 1593, 1500, 1474 (C=C arom.), 1305 (Ge-C arom.), 1149 (C-S-C), 850 (*para*-subst. arom.), 754, 694 (*mono*-subst. arom.). ^{1}H NMR (DMSO-d_6): 10.31 (s, 2H, NH), 7.53–7.51 and 7.34–7.32 (dd, 2H, Ar(H)-S), 7.12–6.73 ppm (m, 18H, Ar(H)-Ge). ^{13}C NMR (DMSO-d_6): 174.3 (C=O), 157.8, 137.0, 136.0*, 133.4, 129.8, 129.4*, 129.2*, 128.9*, 124.4*, 120.8* ppm. $(C_{30}H_{22}N_2O_2SGe)(546.98)_n$: calcd C 65.87%, H 4.02%, N 5.12%; found C 64.96%, H 3.77%, N 4.89%.

Preparation of the polymer–metal composites

High purity gold grains (99.95%) were evaporated by Physical Vapor Deposition (PVD) in high vacuum onto a glass substrate at 20 °C (Scheme 2a-i), which is linked to an Edwards film thickness monitor (model N° FTM5) for controlling the amount of deposited metal. Thus, the gold film thickness was 50 nm. In the same way, sheets of copper pieces (0.01″ thickness) were used for obtaining films of the same thickness. On top of the metal films, 20 μL of pure oil polymers were deposited by spin-coating using rotation speed ramps: 500 rpm about 10 s and 1600 rpm for 10 s. This procedure of incorporation of metal into the polymer matrix is shown in Scheme 2a-ii and Scheme 2a-iii.

Results and discussion

Poly(amides) derived from the 2,5-thiophenedicarboxylic acid (**1**) and two different silicon or germanium-containing aromatic diamines (**2a–b**) were synthesized as shown in Scheme 1. The inclusion of Ge and Si in the repetitive unit produced dark and light brown oil, respectively, which was obtained in good yield (70–73%). The specific structure of repetitive units was verified by FT-IR, NMR (^{1}H, ^{13}C and ^{29}Si) and elemental analyses. The results suggest high purity for the oil samples (Fig. 1).

Solubility of the poly(amides)

The solubility of the polymers at room temperature was tested in various organic solvents. The polymers exhibited a good solubility in a variety of aprotic and protic polar solvents such as dichloromethane, THF, ethyl acetate, acetone, dimethylformamide (DMF), dimethyl sulfoxide (DMSO), *N*,*N*-dimethylacetamide (DMAc), *N*-methyl-2-pyrrolidone (NMP), pyridine, *m*-cresol, ethanol and methanol, but they were insoluble in water. Additionally, the polymers were soluble in non-polar solvents such as $CHCl_3$, Et_2O, toluene and CCl_4 but insoluble in hexane and petroleum ether. The solubility observed for the samples was independent of structural modifications on the repetitive unit.

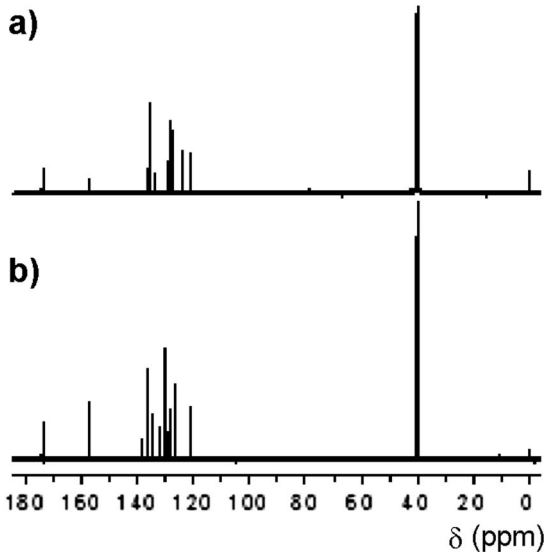

Fig. 1 ^{13}C NMR spectra for pure samples of (a) **PAtGe** and (b) **PAtSi** (400 MHz, DMSO-d_6, 19 °C).

Both poly(amide)s (**PAtSi** and **PAtGe**) showed good film-forming abilities from THF solutions. In all cases, the films were slightly brown in color with good resistance to the manipulation.

Weight molecular-mass fragmentation studies

The effective masses of the poly(amide)s were obtained eluting the sample not more than 22 min at 326 nm wavelength using negative and positive polarity.

The studied polymers showed a range of 33074.2 to 5616.2 *m*/*z* under negative polarity and 47043.6 to 27554.6 *m*/*z* for positive polarity (Table 1), values associated with low-moderate molecular weights. Thus, the oil aspect of the polymer should be related to these molecular weights and also possibly to the specific structure of the repetitive units, because the elemental analysis and the RMN spectra allow discarding the presence of impurities in the samples (Fig. 1). Interestingly, the molecular weight values obtained are higher for **PAtGe** than **PAtSi**. This behavior would be related to the reactivity of the respective monomeric units and, therefore, with the presence of the tetravalent heteroatom. The Ge–C bond is longer than that of Si–C, therefore, the symmetry breaking of the aromatic system inside the germanium-containing diamine allows an increase of its reactivity in the propagation process.

Optical properties

The absorption is indicative of the effective conjugation in the main chain. This behavior is mainly related to the conjugated polymer with short chain length or aromatic cycles such as poly(acetylene),[43,44] poly(aniline)[45] and poly(thiophene) derivatives,[46] among others.

Fig. 2a shows the UV-vis spectra of **PAtGe** and **PAtSi** dissolved in DMSO. These poly(amide)s have a strong absorption in the visible light region. As expected, the maximum absorption peaks are near 327 nm and correspond to π–π* transitions of the neutral polymers. However, one small displacement of the

Table 1 Effective molecular mass obtained by ESI-MASS spectrometry at 326 nm

	Molecular mass weight (*m*/*z*)	
Polymer	Negative mode	Positive mode
PAtGe	33074.2	47043.6
PAtSi	5616.2	27554.6

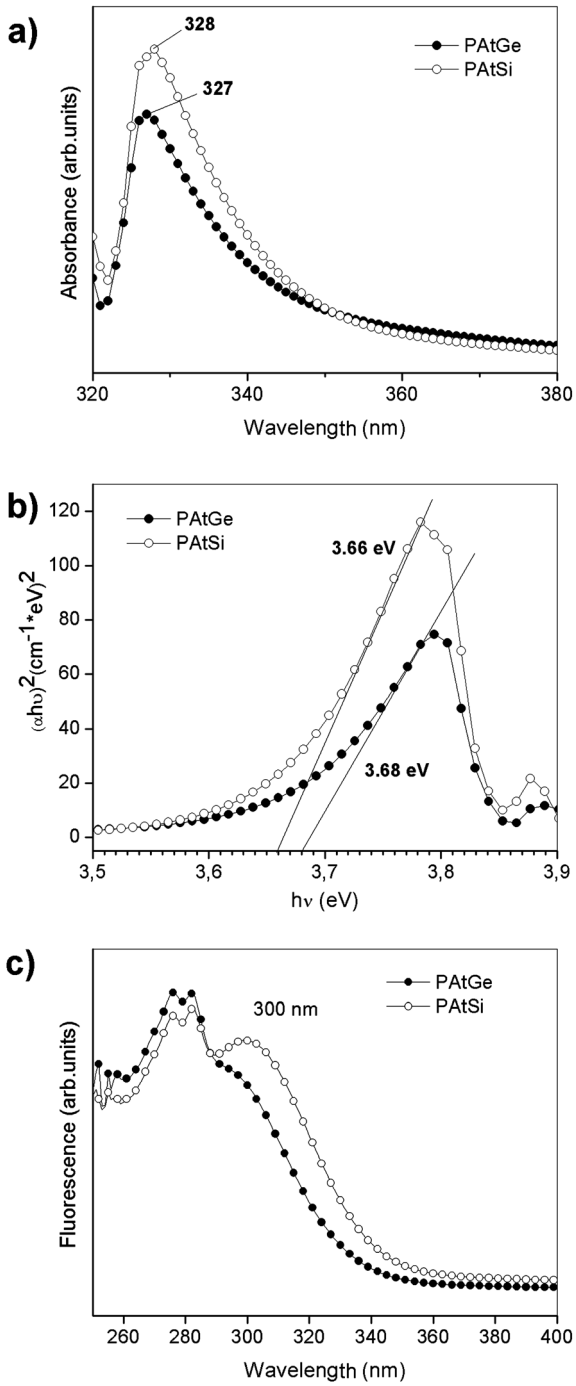

Fig. 2 (a) UV-vis absorption spectra; (b) direct allowed transition energies of poly(amide)s; and (c) fluorescence emission spectra. The spectra of UV-vis were recorded at 25 °C using polymer-DMSO solutions at room temperature.

wavelength between **PAtGe** (327 nm) and **PAtSi** (328 nm) is observable. This fact should be a consequence of the atomic configuration of the inorganic atom into the main chain of the polymer. On the other hand, the longer C–Ge bond in relation to C–Si would promote an important loss of planarity of the chain according to a bigger flexibility in the diamine moiety. This fact would promote a smaller delocalization of electrons in the system. Probably, in our case the polymeric chains have still an appropriate molecular size to observe the conjugation effect.

The optical band gap energy (E_g) in an extended system is defined as the difference between the lowest band energy in the conduction band and the highest band energy in the valence band. The optical absorption coefficient α determines E_g as a function of the photon energy $h\nu$ through the Tauc's expression[47,48] (eqn (1)), where b is a constant.

$$\alpha h\nu = b(h\nu - E_g)^{1/2} \quad (1)$$

The optical absorption coefficient (α) was calculated using eqn (2), which corrects for reflection losses. The parameter A is the absorbance and l the optical path *length* ($l = 1$ cm):[49]

$$\alpha = 2.303(A)/l \quad (2)$$

By plotting $(\alpha h\nu)^2$ *versus* $h\nu$ it is possible to obtain the direct allowed transition energy gap from extrapolation of the linear portion of the plot to the energy axis (Fig. 2b).[48]

The values of band gap for **PAtGe** and **PAtSi** are 3.68 and 3.66 eV (Table 2). This small difference is not related to the presence of the thiophene unit, but rather to the incorporation of Si or Ge and their effect on the coplanarity of the chains just as was mentioned previously. Thus, a bigger electronic conjugation for **PAtSi** is predictable and therefore a smaller value of its band gap.

The fluorescence measurements were made at the 200–500 nm range using fixed excitation and emission slits 10 nm wide (Table 2). The emission peaks of **PAtGe** and **PAtSi** were in the near-UV region (275 and 283 nm). Additionally, **PAtSi** showed a high emission at 300 nm, because the emitting wavelengths depend on its structure (Fig. 2c). The presence of Si within the macromolecular chains produces a shift of the emission maxima toward the UV region. This behavior would agree with the biggest planarity of their chains, which would allow transporting holes and electrons more efficiently. Interestingly, the optical results of **PAtGe** indicate that the π-conjugated system is lower, due probably to the low coplanarity of their chains.

The band gap values around 3.7 eV could be associated with an insulator behavior for these polymers, due to the regioregularity loss of the molecules into the polymeric chain in solution.

Table 2 UV-vis absorption spectra, optical band and fluorescence of the polymers[a]

Polymer	Absorption/nm	Optical band gap/eV	Fluorescence/nm
PAtGe	328	3.68	275, 283
PAtSi	327	3.66	275, 283, 300

[a] Values taken from Fig. 1.

Thermal properties

The thermal properties of the poly(amide)s were evaluated under nitrogen atmosphere by differential scanning calorimetry (DSC) and thermogravimetric analysis (TGA). These results are summarized in Table 3.

The glass transition temperatures were considered as the change in the slopes observed in the DSC thermograms after the second heating run (Fig. 3a). **PAtGe** showed a slightly high T_g value than poly(amide) with Si in the main chain (−59.6 °C and −63.9 °C, respectively). The inverse effect was reported previously for poly(amide) oligomers,[27] where the C–Ge bonds are longer than the C–Si bond, implying a lower rotational barrier in compounds that present Ge in the main chain. Our results can be explained by the higher molecular weight of germanium-containing poly(amide), which was obtained by spectrometric analysis (Table 1). Additionally, this observation can be supported by the diffraction pattern of **PAtGe** that presents a strong intensity peak similar to a semi-crystalline structure, a monoclinic cell (Fig. 5b, X-ray section).

Thermal stability of a polymer depends primarily on the strength of the bonds between the individual atoms and groups forming the macromolecule.[50] As shown in Fig. 3b, the polymers exhibit similar TGA curves. At 170 °C the weight loss is 5% approximately, while at around 240 °C, the samples show a weight loss near 50%. In both cases, the thermal degradation started around 150 °C. In general, a polymer is considered as a thermostable material when a 10% weight loss occurs at a temperature higher than 400–450 °C. In this sense, **PAtSi** and **PAtGe** cannot be considered thermally stable; however, they present an interesting interval of thermal application.

A low content of solid residue at 600 °C (R_{w600}) was obtained in both cases, principally associated with silicon and germanium oxides, respectively.[27,41,51,52]

Raman spectroscopy

Theoretically, a Raman band at 628 cm^{-1} is related to the Cu(1)–O(1)[53,54] system. However, when a thin pure copper film was studied, two vibrations at 607 cm^{-1} and 523 cm^{-1} were found. The band that appears at 607 cm^{-1} has been related to the vibration of oxygen in CuO molecules, while the mode at 520 cm^{-1} is assigned to a phonon of SiO_2 substrate,[54] used as

Table 3 Thermal properties of poly(amide)s containing Ge or Si in their main chain

	Decomposition temperature/°C			DSC
Polymer	T_5[a]	T_{10}[b]	R_{w600} (%)[c]	T_g[d]
PAtGe	165.5	184.6	11.7	−59.6
PAtSi	174.0	196.5	16.4	−63.9

[a] Temperature at which 5% weight loss was recorded by TGA at a heating rate of 20 °C min^{-1} in a nitrogen atmosphere. [b] Temperature at which 10% weight loss was recorded by TGA at a heating rate of 20 °C min^{-1} in a nitrogen atmosphere. [c] Percentage weight of residual material after TGA analysis at temperature 600 °C in a nitrogen atmosphere. [d] Measured from DSC under nitrogen at a heating rate of 20 °C min^{-1}.

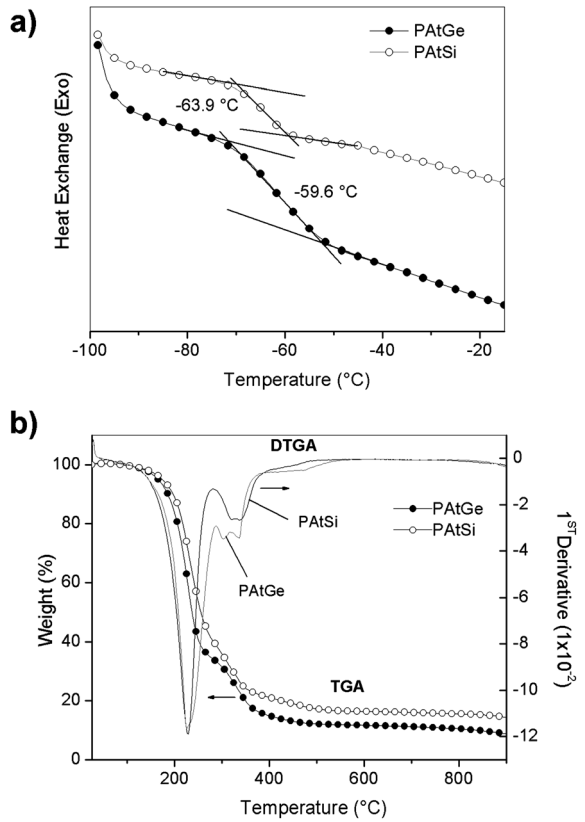

Fig. 3 Thermal analysis for the poly(amide)s: (a) DSC and (b) TGA. Both analyses were recorded at 20 °C min^{-1}, in nitrogen atmosphere.

support for the metal evaporation. On the other hand, the gold film does not exhibit a vibration mode in the Raman spectrum, due to the intrinsic characteristics of the material, a noble metal.

Raman spectra of **PAtSi** (Fig. 4a) exhibit a weak band at 3050 cm^{-1}, due to the aromatic C–H stretching vibration and strong band related to a C–H *in-plane* (*ip*) bending vibration at 995 cm^{-1}. In this last mode, the carbon atoms present an *ip* radial movement, which is the in-phase ring stretching (or "breathing") mode. One band at 1593 cm^{-1}, with a strong intensity, is associated with the C=C ring stretching mode. With respect to the

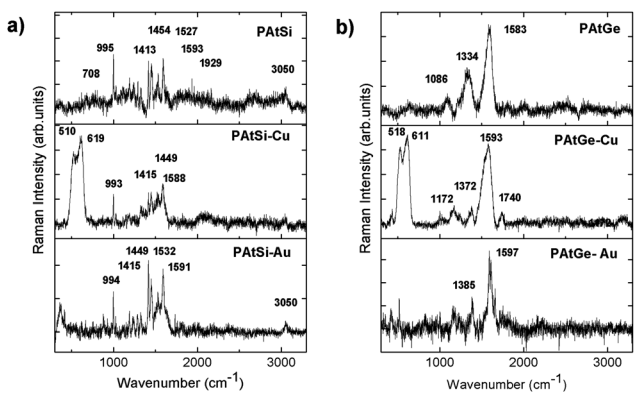

Fig. 4 Raman spectroscopy of pure PAs (**PAtSi** and **PAtGe**) and PAs with incorporation of copper (**PAtSi–Cu** and **PAtGe–Cu**) and gold (**PAtSi–Au** and **PAtGe–Au**).

thiophene moiety, the most intense bands at 1454 cm^{-1} and 1413 cm^{-1} are assigned to the symmetric stretching vibration of the aromatic C=C ring bond. Another interesting band at 1527 cm^{-1} corresponds to the Si–C arom. stretching, while the band at 708 cm^{-1} is related to C–S–C *ip* deformation. On the other hand, the bands that are assigned to the **PAtSi–Cu** composite can be related to the distorted conformation around the silyl group. Thus, this material does not show the band of the C–H stretching around 3050 cm^{-1}, presenting a loss of planarity in the system. However, the band that appears close to 1588 cm^{-1}, associated with C=C ring stretching, is strongly coupled to multi-band systems, such as the case of the Si–C arom. Absorptions at 1530 cm^{-1}, 1415 cm^{-1} and 1449 cm^{-1} correspond to symmetric stretching vibrations of the aromatic C=C of the thiophene ring. The vibration produced by the remainder CuO is assigned to 619 cm^{-1} with a strong intensity compared to the other vibrations, while the band at 519 cm^{-1} is related to the SiO_2 substrate.

On the other hand, the inclusion of gold into the amorphous matrix of the polymer (**PAtSi–Au** composite) showed a band at 3050 cm^{-1} associated with an increase of the crystalline degree. The bands that appear at 1415 cm^{-1} and 1449 cm^{-1} are related to symmetric stretching vibrations of the C=C thiophene ring, while the signs at 1532 cm^{-1} and 1591 cm^{-1} correspond to the Si–C arom. and C=C stretching vibrations, respectively. In comparison to **PAtSi–Cu**, the **PAtSi–Au** composite showed a displacement of Si–C arom. vibration, produced by the disturbance from the electronic distribution of the gold atom.

The **PAtGe** sample presented three vibrational modes with strong, medium and weak intensities at 1583 cm^{-1}, 1334 cm^{-1} and 1086 cm^{-1}, respectively (Fig. 4b). The first band corresponds to the C=C stretching vibration of the aromatic ring. The band at 1334 cm^{-1} possibly can be attributed to two vibrational modes, Ge–C arom. stretching and C–C intra-ring symmetric stretching vibration of the thiophene moiety. Another interesting band, observed at 1086 cm^{-1} in the thiophene ring zone, corresponds to the antisymmetric stretching vibration C–C bonds. On the other hand, the **PAtGe–Cu** composite showed two coupled vibrational modes corresponding to aromatic C=C stretching at 1538 cm^{-1} and 1593 cm^{-1}. Moreover, the bands with weak intensities at 1740 cm^{-1}, 1372 cm^{-1} and 1172 cm^{-1} are related to the C=O *ip* of the amide group, Ge–C arom. stretching or C–C intra-ring symmetric stretching vibration of thiophene and C–O stretching vibrations, respectively. In the Raman spectra of the **PAtGe–Au** composite it is possible to see an amorphous behavior, showing two bands with medium intensities at 1597 cm^{-1} and 1610 cm^{-1} which correspond to the aromatic C=C stretching. In addition, the band at 1385 cm^{-1} with a weak intensity is related to the Ge–C arom. absorption.

X-Ray diffraction analysis

The packing modes of the pure poly(amide)s, **PAtSi** and **PAtGe**, were investigated using X-ray diffraction at room temperature. The samples showed a semi-crystalline pattern evidenced by specific diffraction peaks, indicating a mixture of crystalline and amorphous structures. This idea supports the thermal behavior observed for the samples and their low glass transition temperature (~−64 °C and −60 °C, respectively, Table 3). Thus, at

room temperature it was observed a partial melting of the material, promoting a higher mobility of the polymeric chain. Likewise, the semi-crystalline behavior would be also related to the rigid (phenyl group and thiophene ring moieties) and the flexible moieties (amide group) inside the polymeric chain that would affect negatively the chains packing process.

Thus, the X-ray diffraction patterns of **PAtSi** show a mixture of two monoclinic structures embedded in an amorphous structure (Fig. 5a). Strong diffraction peaks at 9.32° and 18.85° fit the monoclinic structure with the parameters: $\alpha = \gamma = 90°$ and $\beta = 70°$; $a = 5.40$ Å; $b = 5.40$ Å and $c = 10.10$ Å. Low intensity peaks at 20.37°, 21.16°, 22.57° and 25.78° fit the monoclinic structure with the parameters: $\alpha = \gamma = 90°$ and $\beta = 72°$; $a = 5.20$ Å; $b = 5.00$ Å and $c = 9.80$ Å.

Additionally, the inclusion of the metals (Cu or Au) within the polymers was studied.

When the polymer is segregated on a thin copper film (**PAtSi–Cu**), the composite presents a monoclinic lattice embedded in an amorphous structure. A strong diffraction peak at 29.99° and low intensity peaks at 11.03°, 22.24°, 24.29°, 32.35° and 36.21° (Fig. 5a) fit the monoclinic structure with the parameters: $\alpha = \gamma = 90°$ and $\beta = 72°$; $a = 5.10$ Å; $b = 5.05$ Å and $c = 9.30$ Å.

On the other hand, when **PAtSi** was segregated on gold (**PAtSi–Au** composite), the X-Ray analysis showed a mainly amorphous system (Fig. 5a). However, it is possible to distinguish diffraction peaks associated with the monoclinic lattice, which would be embedded in the amorphous matrix. The strong diffraction peak at 25.98° and very low intensity peaks at 19.73°, 21.88° and 38.09° fit the monoclinic structure with parameters: $\alpha = \gamma = 90°$ and $\beta = 72°$; $a = 5.10$ Å; $b = 5.00$ Å and $c = 9.45$ Å.

X-Ray diffraction patterns of the pure **PAtGe** sample show semi-crystalline structures. As shown in Fig. 5b, the strong intensity peaks at 19.12°, 23.58° and 38.97° are associated with a monoclinic cell mixed with an amorphous structure. The low intensity peaks at 11.60°, 20.34°, 33.37° and 35.64° fit the monoclinic structure with the parameters: $\alpha = \gamma = 90°$ and $\beta = 72°$; $a = 4.85$ Å, $b = 4.90$ Å and $c = 8.00$ Å.

When the polymer was segregated on a thin copper film (**PAtGe–Cu** composite), the X-ray diffraction patterns showed also a similar semi-crystalline structure (Fig. 4b). The strong diffraction peaks at 14.18° and 21.55° and the low intensity peaks at 11.79°, 19.40°, 23.62°, 26.35°, 28.91° and 32.55° fit the monoclinic structure with the parameters: $\alpha = \gamma = 90°$ and $\beta = 72°$; $a = 5.10$ Å, $b = 5.80$ Å and $c = 7.90$ Å.

A **PAtGe** polymer segregated on Au allows obtaining a **PAtGe–Au** composite. X-Ray analysis of this material shows a mainly amorphous behavior. However, strong diffraction peaks at 19.97° and 38.34° are observed, which fit the monoclinic structure with parameters: $\alpha = \gamma = 90°$ and $\beta = 72°$; $a = 4.96$ Å, $b = 5.80$ Å and $c = 7.95$ Å.

Table 4 summarizes the data of the pure polymers and composites (polymer–metal) obtained by XRD. All compounds showed the same phase with a certain degree of amorphousness. However, polymer–Au composites revealed the presence of well-defined elongation of the structure compared with the polymer–Cu composites. This effect might be related to the coordination between the Au and the central atoms of the poly(amide)s (Si or Ge), which produces a distortion of the unit cell.

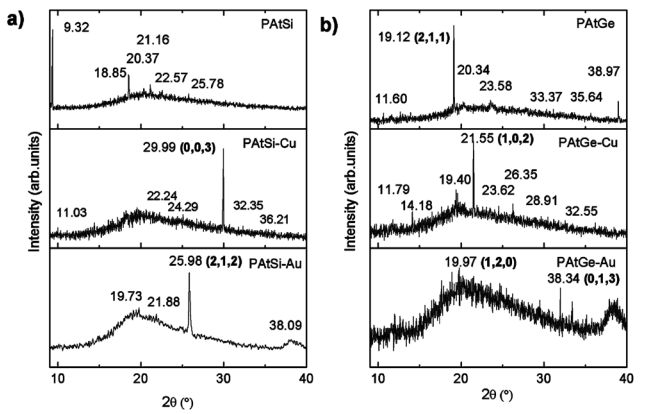

Fig. 5 Wide angle X-ray diffractograms with Miller indexes of poly(amide)s: (a) **PAtSi** with/without metal and (b) **PAtGe** with/without metal.

Conductivity measurement: current–voltage curve

In order to study the inclusion of the metals into the polymeric matrix, 50 nm thick films of Au and Cu were deposited separately on glass substrates by physical vapor deposition (PVD). Then, pure oil-polymers were deposited on top of the metal films by spin-coating as shown in Scheme 2a-ii. To measure the current, two electrodes, separated by 2 mm (d), were inserted to the drop, touching the glass substrate (Scheme 2b). This systematic and reproducible procedure was performed on both pure polymers and polymer–metal composites and their results are shown in Fig. 6.

For both polymeric systems, the conductance increased with the inclusion of the metals. Thus, the **PAtSi–Au** composite showed a conductance one order of magnitude higher than that of the **PAtSi–Cu** composite and **PAtSi** alone (Fig. 6a). Likewise, the **PAtGe–Au** sample showed a conductance one order of magnitude higher than that of the **PAtGe–Cu** composite and two orders of magnitude higher than that of pure **PAtGe** (Fig. 6b).

The conductivity changes in the polymer–metal composites are related to Coulomb interactions between the charge of the main chain of the polymers and the dopant ions, which modify the band gap value. Additionally, percolation field effects[32–35] might arise in the polymer–Au composites (**PAtSi–Au** and **PAtGe–Au**), which would be characterized by metallic islands separated by beaches of insulator polymer (conductivity of 1.24×10^{-6} and 1.7×10^{-7} S cm^{-1}, respectively). Thus, the increase of the conductivity with respect to pure samples would be related to the extension of electrical percolation between the proposed metallic islands and the insulator polymer. This effect was not observed for the polymer–Cu composites probably due to the higher dispersion of the Cu island into the polymeric matrixes, prevailing in this way, the insulating characteristics of the polymer.

The conductivity v s^{-1} voltage curves shown in Fig. 6a demonstrate a characteristic diode behavior, with a ratio of rectification higher for the **PAtSi–Au** composite than **PatSi** alone. This fact would be due to the inclusion of the metal into the polymer, which would reduce the resistance of the system in one direction. This interesting behavior implies that further increase of the conductivity might be controlled by either synthesis or inclusion parameters. Although more studies are

Table 4 X-Ray powder diffraction

Polymeric system	Structure	$\alpha = \gamma$/deg	β/deg	a/Å	b/Å	c/Å
PAtSi	Monoclinic (strong intensity peak)	90	70	5.40	5.40	10.10
	Monoclinic (low intensity peak)	90	72	5.20	5.00	9.80
PAtSi–Cu	Monoclinic (strong/low diffraction peak)	90	72	5.10	5.05	9.30
PAtSi–Au	Monoclinic (strong/low diffraction peak)	90	72	5.10	5.00	9.45
PAtGe	Monoclinic (strong/low diffraction peak)	90	72	4.85	4.90	8.00
PAtGe–Cu	Monoclinic (strong/low diffraction peak)	90	72	5.10	5.80	7.90
PAtGe–Au	Monoclinic (mainly amorphous)	90	72	4.96	5.80	7.95

needed in order to develop doped-polymer semiconductors from these polymeric materials, some interesting applications in the electronic field could be suggested based on the current results.

Scanning electronic microscopy (SEM)

Fig. 7 shows the scanning electron microscopy images of the surface of the polymer–metal composite films at 5 kV magnification voltages. In this figure, poly(amide)s with thiophene moiety do not show capsulation of the metal. In addition, the surface morphology of the composites presents irregularities for different polymer–metal aggregates. This fact suggests that the polymer can stabilize the metallic particles through coordination with the sulfur atom of the repetitive unit.

For the inclusion of copper in the polymeric matrix, a high superficial agglomeration is evident (Fig. 7a and c) compared to the gold inclusion (Fig. 7b and d). This behavior could be related to the smaller atomic radius of copper, which produces a diminution in the inter-separation of the polymer–metal system.

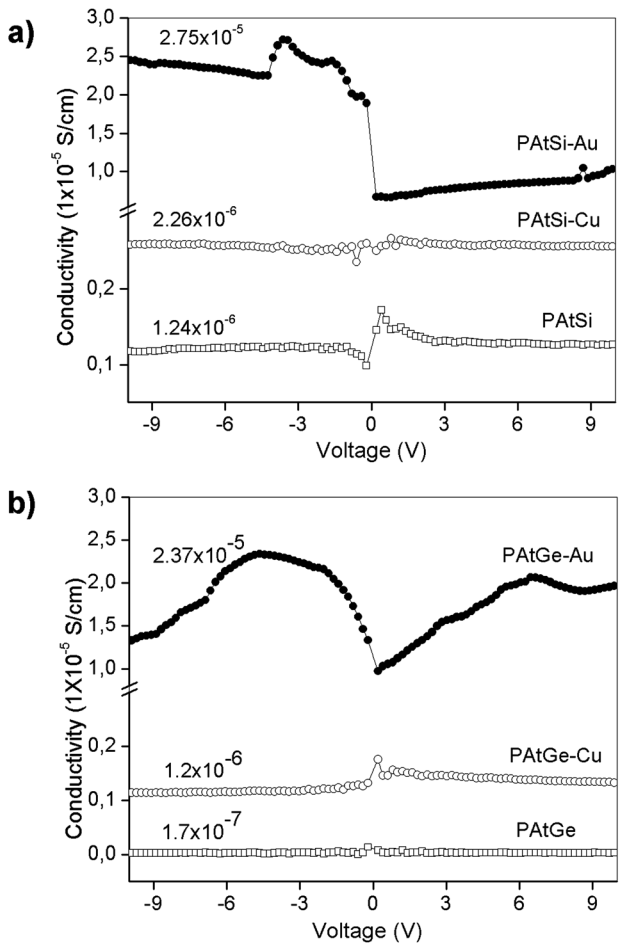

Fig. 6 Electrical conductivity of the polymers and the polymer–metal composites based on: (a) **PAtSi** and (b) **PAtGe**.

Size effect of the metallic particles on the electrical and optical properties of the polymer–metal composites

The conductivity and the displacement of the surface gold plasmon resonance were studied by the "four-point method" and UV-vis spectroscopy in the solid state, respectively (Fig. 8). For this purpose, we prepared five different polymer–gold composites modifying the polymeric concentration: 0.700; 0.230; 0.110; 0.077 and 0.058 g of **PAtSi** or **PAtGe** in 1 mL of DMSO and using gold films with a constant thickness of 50 nm. These analyses allow us to estimate the influence of the particle shape and packing density on the electrical conductivity of the composites, explaining the gold percolation effect on polymeric matrixes.

Fig. 8 shows that the conductivity values changed over several orders of magnitude, according to the amount of polymer deposited on the metallic films. The tendency observed is similar in composites derived from **PAtSi** (Fig. 8a) or **PAtGe** (Fig. 8b) and shows that for a high inclusion of the metal into the polymeric matrix, the conductivity of the composites increases significantly.

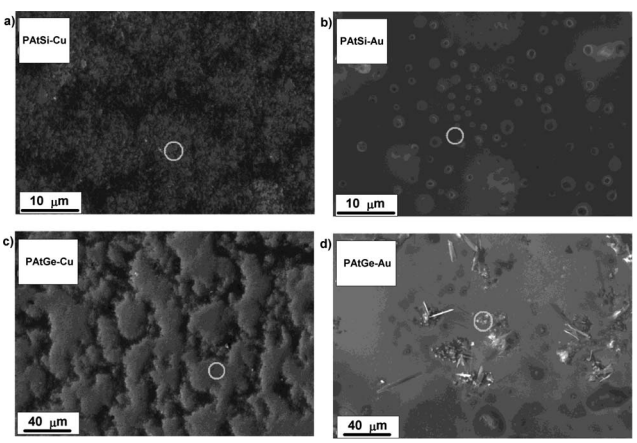

Fig. 7 SEM micrographs of polymer–metal composite films.

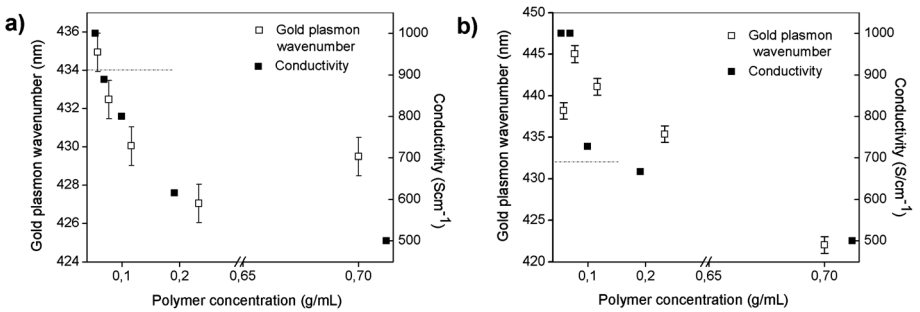

Fig. 8 Dependence of electrical conductivity on the amount of metallic particles in the polymer matrix: (a) **PAtSi–Au** and (b) **PAtGe–Au**.

On the other hand, the optical properties were also studied as a function of the composition of the polymer–metal composites, observing the displacement of the so-called surface plasmon resonance or particle plasmon resonance (PPR) (Fig. 8). When the composite is excited by light, photons are coupled at the metal interface causing an induced charge density oscillation that creates a strong absorption maximum at a particular wavelength. The position of the absorption maximum depends on the cluster size, shape and particle distance as well as on the polymeric concentration.

The absorption spectrum of a pure gold film shows one typical band with a shoulder at 434 nm, related to the surface plasmon resonance band. Thus, the displacement of this wavelength is associated with a decrease or increase of the particle size.[55]

Fig. 8 shows that the decrease in the polymer concentration (**PAtSi** or **PAtGe**) on the gold film produces random segregated systems increasing the conductivity of the polymer–metal composites. In fact, this behavior also is related to the particles shape and it influences the packing density, which is observed by the displacement at a lower wavelength of the gold plasmon band. On the other hand, a higher polymer concentration allows the formation of shell structures isolating the metallic particles, which produce lower conductivities, decreasing the wavelength of the gold plasmon band.

Conclusions

The synthesis of two poly(amide)s (**PAtGe** and **PAtSi**) was realized. TPP, $CaCl_2$ and Py in an NMP system was effectively applied for the direct polycondensation of 2,5-thiophenedicarboxylic acid and two aromatic diamines, containing Si or Ge in the central part of the molecule. The resulting poly(amide)s exhibited a good solubility in a variety of polar and apolar organic solvents. Asymmetry factors and steric hindrance within the repetitive unit prevent dense packing of the chain and lead to a decrease of the glass transition temperature and thermal stability, also resulting in an insulator behavior, associated with a large band gap. The results of effective molecular mass of the polymers were related to the reactivity of the heteroatoms. The X-ray diffraction patterns of the polymers and polymer–metal composites showed a mixture of monoclinic and amorphous structures. The inclusion of Au and Cu atoms into the pure polymers produces a distortion of the unitary cell probably due to the coordination between the central atoms of the main chain (Si or Ge) and the metal atom studied. On the other hand, the inclusion of the metal into a polymer matrix was investigated experimentally. An increase up to two orders of magnitude in the conductance was obtained for polymer–Au composites, probably due to the homogeneous distribution of the Au atoms into the polymeric matrix. Polymer–Cu composites showed a lower conductance, due to the heterogeneous distribution of the Cu atoms, which would produce structural anisotropies. In this context, the formation of metallic clusters should be considered as an important mechanism for the electrical behavior of these novel systems. Finally, the inclusion of Au into **PAtSi** produced a diode-like behavior, which was demonstrated to operate at a specific voltage (*e.g.* compared to the band gap, *etc.*).

The polymer–metal composites reveal synergism of properties of the initial components (gold and polymer), which produce specific electrical and optical properties, related to an ordered distribution of metallic particles in the polymer matrix. Thus, when the polymer concentration decreases, the new material exhibits properties specifically related to the metal, behavior supported by the formation to a metal–particle aggregation with a higher size.

Acknowledgements

C. M. González-Henríquez acknowledges a Scholarship from MECESUP UCH 0601 and the corresponding authors thank the financial support provided by FONDECYT project: Nr 1095151, 1100015 and 1100882. Thanks to M. Pavez Moreno for the conductivity measurements.

References

1 S. B. Oh, Y. K. Choi and C. S. Cho, *J. Appl. Polym. Sci.*, 2003, **88**(11), 2649.
2 C. G. Granqvist, A. Azens, J. Isidorsson, M. Kharrazi, K. Kullman, T. Lindström, G. A. Niklasson, C. G. Ribbing, D. Rönnow, M. M. Strømme and M. Veszelei, *J. Non-Cryst. Solids*, 1997, **218**, 273.
3 H. J. Byker, Gentex Corporation, *US Pat.* 4902108, 1990.
4 R. G. Mortimer, *Chem. Soc. Rev.*, 1997, **26**, 147.
5 P. M. S. Monk, *J. Electroanal. Chem.*, 1997, **432**, 175.
6 K. Bange, *Sol. Energy Mater. Sol. Cells*, 1999, **58**, 1.
7 C. G. Granqvist, A. Azens, A. Hjelm, L. Kullman, G. A. Niklasson, C. G. Ribbing, D. Roennow, M. M. Stromme, M. Veszelei and G. Vaivars, *Sol. Energy*, 1998, **63**, 199.
8 R. D. Rauh, *Electrochim. Acta*, 1999, **44**, 3165.
9 C. E. Tracy, J. G. Zhang, D. K. Benson, A. W. Czanderna and S. K. Deb, *Electrochim. Acta*, 1999, **44**, 3195.
10 A. Pennisi, F. Simone, G. Barletta, G. Di Marco and M. Lanza, *Electrochim. Acta*, 1999, **44**(18), 3237.

11 D. L. Meeker, D. S. K. Mudigonda, J. M. Osborn, D. C. Loveday and J. P. Ferraris, *Macromolecules*, 1998, **31**(9), 2943.
12 D. S. K. Mudigonda, D. L. Meeker, D. C. Loveday, J. M. Osborn and J. P. Ferraris, *Polymer*, 1999, **40**, 3407.
13 I. D. Brotherston, D. S. K. Mudigonda, J. M. Osborn, J. Belk, J. Chen, D. C. Loveday, J. L. Boehme, J. P. Ferraris and D. L. Meeker, *Electrochim. Acta*, 1999, **44**, 2993.
14 D.-J. Liaw, F.-C. Chang, M.-K. Leung, M.-Y. Chou and K. Muellen, *Macromolecules*, 2005, **38**(9), 4024.
15 D. J. Liaw and B. Y. Liaw, *Macromol. Symp.*, 1997, **122**, 343.
16 D. J. Liaw, P. N. Hsu, W. H. Chen and S. L. Lin, *Macromolecules*, 2002, **35**(12), 4669.
17 M. Ballauff and G. F. Schmidt, *Makromol. Chem. Rapid Commun.*, 1987, **8**, 93.
18 M. Steuer, M. Hörth and M. Ballauff, *J. Polym. Sci., Part A: Polym. Chem.*, 1993, **31**(6), 1609.
19 L. Cheng and X. G. Jian, *J. Appl. Polym. Sci.*, 2004, **92**, 1516.
20 M. Yamada, M. Kusama, T. Matsumoto and T. Kurosaki, *Macromolecules*, 1993, **26**(18), 4961.
21 M. Kusama, T. Matsumoto and T. Kurosaki, *Macromolecules*, 1994, **27**, 1117.
22 D. J. Liaw, B. Y. Liaw, P. N. Hsu and C. Y. Hwang, *Chem. Mater.*, 2001, **13**(5), 1811.
23 D. J. Liaw, B. Y. Liaw and C. M. Yang, *Macromolecules*, 1999, **32**(21), 7248.
24 Y. Liang, D. Feng, J. Guo, J. M. Szarko, C. Ray, L. X. Chen and L. Yu, *Macromolecules*, 2009, **42**(4), 1091.
25 L. Zhanga, Q. Zhang, H. Rena, H. Yan, J. Zhang, H. Zhang and J. Gu, *Sol. Energy Mater. Sol. Cells*, 2008, **92**(5), 581.
26 J.-Y. Lee, W.-S. Shin, J.-R. Haw and D.-K. Moon, *J. Mater. Chem.*, 2009, **19**, 4938.
27 L. H. Tagle, C. A. Terraza, A. Leiva and P. Alvarez, *e-Polym.*, 2009, **34**, 1.
28 M. Bruma and B. Schulz, *J. Macromol. Sci., Part C: Polym. Rev.*, 2001, **41**(1 and 2), 1.
29 I. Sava, M. Szesztay, M. Bruma, F. Mercer and B. Schulz, *Angew. Makromol. Chem.*, 1997, **253**, 169.
30 S. F. Thames and K. G. Panjnani, *J. Inorg. Organomet. Polym.*, 1996, **6**(2), 59.
31 C. M. González-Henríquez, L. H. Tagle, C. A. Terraza, A. Barriga González, U. G. Volkmann, A. L. Cabrera, E. Ramos-Moore and M. Pavez-Moreno, *Polym. Int.*, 2012, **61**, 197.
32 B. Lin, G. A. Gelves, J. A. Haber and U. Sundararaj, *Ind. Eng. Chem. Res.*, 2007, **46**(8), 2481.
33 S. I. White, P. M. Vora, J. M. Kikkawa, J. E. Fischer and K. I. Winey, *J. Phys. Chem. C*, 2010, **114**, 22106.
34 A. Buffet, M. M. M. A. Kashem, K. Schlage, S. Couet, R. Röhlsberger, A. Rothkirch, G. Herzog, E. Metwalli, R. Meier, G. Kaune, M. Rawolle, P. Müller-Buschbaum, R. V. Gehrke and S. Roth, *Langmuir*, 2011, **27**(1), 343.
35 M. Mu, M. E. Seitz, N. Clarke, R. J. Composto and K. I. Winey, *Macromolecules*, 2011, **44**(2), 191.
36 M. Muccini, *Nat. Mater.*, 2006, **5**, 605.
37 M. C. Lechman, D. Kessler and J. S. Gutman, *Langmuir*, 2009, **25**, 10202.
38 S. Ki, J. R. Jinschek, H. Chen, D. S. Scholl and E. Marand, *Nano Lett.*, 2007, **7**(9), 2806.
39 L. H. Tagle, F. R. Díaz, D. Radic, A. Opazo and J. M. Espinoza, *J. Inorg. Organomet. Polym.*, 2000, **10**(2), 73.
40 J. Pratt and S. F. Thames, *J. Org. Chem.*, 1973, **38**(25), 4271.
41 A. Tundidor-Camba, C. A. Terraza, L. H. Tagle and D. Coll, *J. Appl. Polym. Sci.*, 2011, **120**, 2381.
42 N. Yamazaki, M. Matsumoto and F. Higashi, *J. Polym. Sci., Polym. Chem. Ed.*, 1975, **13**, 1373.
43 M. Lögdlund, W. R. Salaneck, F. Meyers, J. L. Brédas, G. A. Arbuckle, R. H. Friend, A. B. Holmes and G. Froyer, *Macromolecules*, 1993, **26**, 3815.
44 K. Ziemelis, *Nature*, 1998, **393**, 619.
45 A. J. Heeger, *Angew. Chem., Int. Ed.*, 2001, **40**, 2591.
46 T. Ahn, B. Choi, S. H. Ahn, S. H. Han and H. Lee, *Synth. Met.*, 2001, **117**, 219.
47 J. Tauc, R. Grigorovici and A. Vancu, *Phys. Status Solidi B*, 1966, **15**, 627.
48 J. Tauc, *Mater. Res. Bull.*, 1968, **3**, 37.
49 F. Mark, *Optical Properties of Solids*, Oxford University Press Inc, New York, 2001.
50 E. N. Guŕyanova, *Russ. Chem. Rev.*, 1968, **37**(11), 863.
51 L. H. Tagle, C. A. Terraza, A. Leiva, N. Yazigi and L. López, *J. Appl. Polym. Sci.*, 2010, **117**, 1526.
52 C. A. Terraza, L. H. Tagle and A. Leiva, *Polym. Bull.*, 2009, **63**, 663.
53 N. Kazuo, *Infrared and Raman Spectra of Inorganic and Coordination Compounds: Part A: Theory and Applications in Inorganic Chemistry*, John Wiley & Sons, Inc, New York, 5th edn, 1997, pp. 155.
54 S. Hong, H. Cheong and G. Park, *Phys. C*, 2010, **470**, 383.
55 U. Kreibig and M. Vollmer, *Optical Properties of Metal Clusters, Volume 25 of Springer Series in Materials Science*, Springer-Verlag, Berlin, 1995.